

# The impact of deforestation on the hydrological cycle in Amazonia as observed from remote sensing

Noemi Vergopolan <sup>a,b</sup> and Joshua B. Fisher <sup>c</sup>

<sup>a</sup>Department of Environmental Engineering, Federal University of Parana, Curitiba, Brazil; <sup>b</sup>Department of Civil and Environmental Engineering, Princeton University, Princeton, NJ, USA; <sup>c</sup>Jet Propulsion Laboratory, California Institute of Technology, Pasadena, CA, USA

## ABSTRACT

Given widespread Amazonian deforestation, numerous studies have focused on how the regional hydrological cycle – in terms of precipitation ( $P$ ) recycling from evapotranspiration (ET) – is impacted by deforestation. Nevertheless, climate macroscale and mesoscale models have given contradictory results on changes in ET and  $P$  with deforestation. To date, these results have not been evaluated with observations, so in this work, we assessed a decade of patterns in ET and  $P$  over deforested and forest areas using remote sensing (MODIS and TRMM, 2000–2012). We found a relative increase in ET and  $P$  in deforested areas, though there was a positive ET and  $P$  correlation over southern/deforested, and negative in northern/forested Amazonia. Although the absolute ET and  $P$  values are lower in deforested areas in comparison to border areas, we observed a positive change in ET and  $P$  in the last 10 years at the deforested areas. The increase in ET was larger within the deforested areas; meanwhile,  $P$  increased more from inside forest areas to the borders, which agrees with the ET and  $P$  correlation patterns. Our results help to inform the debate between the macroscale and mesoscale models, as deforestation impacts small-scale circulation patterns, turbulence, and moisture fluxes and convergence, and expand our understanding of the processes involved.

## ARTICLE HISTORY

Received 10 December 2015  
Accepted 30 August 2016

## 1 Introduction

Home to the largest biodiversity on the planet, the Amazon rainforest also impacts the regional precipitation, runoff, and evapotranspiration, as well as global moisture air mass fluxes (Marengo et al. 2012; Randow et al. 2012; Lewis et al. 2011; Fisher et al. 2009). The rainforest can impact various aspects of the surrounding climate, including cloud coverage, heat absorption, and rainfall, but it also influences large-scale circulation acting as a driver of regional climate change in the extratropics (Medvigy et al. 2013). With widespread tropical deforestation, numerous studies have focused on how the regional/local hydrological cycle – specifically precipitation ( $P$ ) recycling from evapotranspiration (ET) – is impacted by deforestation (Nobre et al. 2009; Aragao et al. 2008; Costa and Pires

**CONTACT** Noemi Vergopolan  [noemi@princeton.edu](mailto:noemi@princeton.edu)  Federal University of Parana, Curitiba, PR, Brazil

 The supplemental data for this article can be accessed [here](#)

© 2016 Informa UK Limited, trading as Taylor & Francis Group

2010). The link between ET and  $P$  in Amazonia is central to these teleconnections, particularly because deforestation alters ET, as forests exert control over the timing and magnitude of ET (Spracklen, Arnold, and Taylor 2012; Randow et al. 2012), and associated shifts in  $P$  can strengthen hydrological changes in the short and long terms.

The impacts of Amazonian deforestation on local and global hydrological cycle are of critical importance, and this topic has addressed by numerous modelling studies. However, there remains a divide in these studies on the impact of deforestation on  $P$  and ET in Amazonia. On one side are coarse scale ( $1^{\circ}$ – $5^{\circ}$ ) global/mesoscale climate models, which show an increase in surface air temperature and a decrease in local  $P$ , ET, moisture convergence, and runoff with deforestation (D’Almeida et al. 2007; Dickinson and Kennedy 1992; Eltahir and Bras 1996; Shukla, Nobre, and Sellers 1990). Nonetheless, because of the grid size and parameterizations used, these models have not been able to accurately reproduce the surface temperature gradients in heterogeneous areas (Knox et al. 2011; Garcia-Carreras and Parker 2011). Instead, local thermally driven convection is superseded by subgrid-scale parameterizations, which represent convection and micro-physical cloud processes based on the large-scale mean state of the atmosphere (Molinari and Dudek 1992). Thus, the land–atmosphere interactions necessary for accurately simulating the region hydroclimate are not well resolved in these models (Ramos da Silva and Avissar 2006).

On the other side are relatively fine scale ( $<1^{\circ}$ ) mesoscale models, which have shown an opposite pattern to the macroscale models – an increase in  $P$  (along the borders between forest and deforested/urban areas) and an increase (though also sometimes a consistent decrease) in ET with deforestation depending on the deforestation extent (Knox et al. 2011; D’Almeida et al. 2007; Roy and Avissar 2002). These contradictory results from the mesoscale models result from their detailed hydrological response to deforestation and skill in capturing horizontal heterogeneity in the turbulent surface. An accurate representation of the energy fluxes is important because sensible and latent heat fluxes can induce local thermally driven circulation, and increase local convection and formation of shallow cumulus clouds, strengthening mesoscale circulations (Roy and Avissar 2002; Negri et al. 2004; Knox et al. 2011).

These studies have largely focused on modelling experiments, yet few studies used direct, regional-scale, remote-sensing observations of the hydrological cycle against deforestation over Amazonia. Remote-sensing products based on satellite observations provide a good spatial coverage at a higher resolution in comparison to macro- and mesoscale models, and are able to delineate fine-scale physical processes that are often parameterized by large-scale models. Azarderakhsh et al. (2011) carried out one of the few studies to diagnose the components of the Amazonian water budget and spatio-temporal variability using monthly averaged remote-sensing-based data products. They found that there were opposite sign anomalies of  $P$  and ET in Amazonia. However, they did not assess directly the hydrological impact against deforestation, and, as such, they used a short time interval of analysis (2002–2006).

Similarly, Aragao et al. (2008) analysed satellite-derived monthly and annual time series of rainfall, fires, and deforestation (INPE-DETER and INPE-PRODES) to quantify the seasonal patterns and relationships between these three variables. Through a spectral analysis, they showed that the relationship between anomalies  $P$  and deforestation had a phase shift of approximately  $\pi/2$ , which indicates that the peak of rainfall precedes the

deforestation peak by three months; still, the second deforestation peak in the power spectra coincides with the peak of the dry season.

Finally, Knox et al. (2011) investigated how  $P$  frequency changes as a function of distance to the forest's edge, using  $P$  from TRMM and a land-cover classification from MODIS to address the deforestation impacts. They found that  $P$  frequency decreases over deforested areas far removed (10-plus km) from forest borders, but increases over the forest edge, particularly over the deforested side of the transition. Nevertheless, this analysis was restricted to the southwestern Amazonia, and only evaluated the afternoon precipitation on the dry season (June–October).

Towards a more comprehensive approach designed to improve understanding of the hydrological impacts from deforestation throughout the entire Amazon basin, and inform macroscale and mesoscale modellers on changes in ET and  $P$  associated with deforestation, our study assessed how land-use and land-cover changes affect water cycle dynamics by using a remote-sensing approach that addressed deforestation impacts at seasonal timescales. The focus is mainly on ET and  $P$  changes and differences between forest and deforested areas. The specific objectives of this study are: (1) to identify differences in ET and  $P$  from intact forest, border and deforested areas; and, (2) to evaluate relationships between ET and  $P$  Amazon-wide.

## 2. Materials and methods

As ET and  $P$  are the two largest components in the global terrestrial water cycle (Pokam, Djiotang, and Mkankam 2012; Spracklen, Arnold, and Taylor 2012), a preliminary analysis was performed to identify dynamic changes in ET and  $P$  due to changes in vegetation cover. This analysis compares deforested pixels versus the closest non-deforested at the pixel level, then integrated for the Amazon basin.

For land-cover type we used the Land Cover Type Yearly Climate Modeling Grid (CMG) product. This product has a  $0.05^\circ$  spatial resolution and provides the dominant land-cover type as well as the sub-grid frequency distribution of land-cover classes using the International Geosphere Biosphere Programme (IGBP) classification scheme. To address changes in hydrological dynamics, we reclassify/simplify this to a forest/deforested. 'Forest areas' included evergreen, deciduous, and mixed forest; the remaining non-forest areas that were not waterbodies (as croplands, urban areas, permanent wetlands, grasslands, cerrado, and possible recovering areas) were classified as 'deforested areas'. Nonetheless, we used a tropical rainforest mask (Soares-Filho et al. 2006) to differentiate the majority of natural non-forest areas as cerrado.

For instance, when identifying deforested areas from land-cover type, we observed that evergreen broadleaf forest used to represent 74.6% of the vegetation in 2001 but it decreased to 72.6% in 2011. The classified deforested areas, however, increased from 25.4% in 2001 to 27.4% in 2011, in which savannas only accounts for 10% of the total area. Detailed maps of the classified 'deforested areas' between 2001 and 2011, and the yearly increase in classified 'deforested' pixels are shown in Figures S1–S3 in the Supplemental Material.

Once we determined the deforested pixels for each year, we also identified its nearest forest (border) pixels and the second nearest forest (here called intact forest) pixels. The border pixels were selected through a pixel-to-pixel verification: for a given deforested

pixel, it was selected from all the forest pixels among its eight surrounding pixels. Similarly, the intact forest pixels were selected among the eight surrounding forest pixels of a border pixel.

We used the ET data set from MOD16 (Mu et al. 2007; Mu, Zhao, and Running 2011) and the  $P$  from Tropical Rainfall Measuring Mission 3B43 (TRMM). The MOD16 algorithm is based on the Penman–Monteith equation (Monteith 1965) and accounts for both surface energy partitioning and environmental constraints on ET; it includes canopy interception, evaporation from wet/moist soil surfaces, and transpiration through vegetation pores (stomata). It is computed globally using MODIS land-cover and leaf area index (LAI), albedo, and fractional absorbed photosynthetically active radiation (PAR) as remote-sensing variables. MOD16 uses global surface meteorological variables as air pressure, air temperature, air humidity, and radiation from NASA/GMAO – Global Modeling and Assimilation Office (GMAO) – Modern Era Retrospective Analysis (MERRA) at  $0.5^\circ \times 0.66^\circ$  resolution. Proportional vegetation cover is derived from MODIS fractional absorbed photosynthetically active radiation (fPAR) and enhanced vegetation index (EVI) product (MOD13A2) (Los 1999) is used to partition net radiation ( $R_n$ ) between vegetation and soil surfaces. Leaf-level stomatal conductance is determined by the mean daytime surface air vapour pressure deficit ( $D_a$ ) and daily minimum air temperature ( $T_{amin}$ ), and further up-scaled to the non-wet canopy level using the MODIS LAI product (MOD15A2). The MOD16 data set has a fine temporal resolution of 8 days with  $0.5^\circ$  (5.6 km) spatial resolution and coverage from 2000 to 2012.

Extensive evaluations have been conducted throughout the literature on the MOD16 product (e.g. Miralles et al. (2015)). While instantaneous and daily ET values tend to show relatively high bias, when values are integrated at monthly, seasonally, or yearly time-scale, the MOD16 product has demonstrated a potential for spatial and temporal monitoring of the ET process (Ruhoff et al. 2013b; Trambauer et al. 2014), especially in providing an operational product at mesoscales scales (Srivastava et al. 2016), where little or no gauged data exist. Comprehensive validations have been done within the Amazon basin to address uncertainties in the ET estimation. Specifically, Mu, Zhao, and Running (2011), Ruhoff (2011), and Ruhoff et al. (2013a) validated the product at multiple eddy covariance FLUXNET sites throughout Amazonia. At one of the towers, Mu, Zhao, and Running (2011) found an average daily ET of  $3.08 \text{ mm day}^{-1}$  with a mean bias of  $-0.44 \text{ mm day}^{-1}$ ; correlation coefficient and Taylor skill scores were 0.76 and 0.64, respectively. At another tower, the average daily ET was  $3.63 \text{ mm day}^{-1}$  with a mean bias of  $-0.29 \text{ mm day}^{-1}$ ; correlation coefficient and Taylor skill scores were 0.62 and 0.65, respectively. In a complementary analysis of Mu, Zhao, and Running (2011), Ruhoff (2011) and Ruhoff et al. (2013a) compared 6 years' average annual ET from seven flux towers in different regions in the Amazon, and the analysis resulted in a mean error of  $11 \pm 6\%$ , and an average difference of 6% over the 6 years (see Ruhoff (2011) for details). These results are in agreement with Sun et al. (2007) and Trambauer et al. (2014), and highlight the ability of the MOD16 algorithm for applications in the Amazon rainforest. As such, we use the extensive validation work available in the scientific literature to place uncertainty bounds on our analysis, which allow us to evaluate statistical significance in our findings.

In terms of spatial variability and coverage, MODIS products have been the widely used for studies of Amazonia due to the improved data quality when compared to

AVHRR (Huete et al. 2000, 2002). MOD16 can be used to address hydrological changes due to deforestation, since it has been shown to provide reasonable ET estimates to capture temporal dynamics in environments undergoing chronic disturbances (Knipper, Kinoshita, and Hogue 2016). Regardless of the absolute errors associated with MOD16, our analysis focuses on relative differences between forest and deforested areas, so the impact of the absolute error is minimized here.

To compare MOD16 ET and TRMM  $P$ , it was necessary to either decrease ET resolution from  $0.05^\circ$  to  $0.25^\circ$  or increase  $P$  from  $0.25^\circ$  to  $0.05^\circ$ . Increasing the TRMM resolution can cause the same  $P$  values to correspond with different ET values for the same area, losing spatial correlation power. Therefore, we downscaled the ET data set to  $0.25^\circ$ . We acknowledge that while the  $0.25^\circ$  resolution is a coarse spatial scale to address individual boundary changes, when it is averaged together we may be able to distinguish gradients in ET and  $P$  over forest borders at large. However, it is not our goal to address edge effects, but rather compare undisturbed, relatively homogeneous regions to those with fragmented forest areas. Thus, this resolution demonstrated to be sufficient to identify eminent signals and address changes in the hydrological dynamics in comparison to modelling studies.

The TRMM 3B43 data set contained the best-estimate  $P$  rate and root-mean-square (RMS)  $P$ -error estimate field (3B43) by combining the 3-hourly merged high-quality/IR estimates with the monthly accumulated Global Precipitation Climatology Centre (GPCC) rain gauge analysis. Karaseva, Prakash, and Gairola (2012) and Ramos da Silva, and Avissar (2008) reported that the TRMM product performed reasonably well over plain and orographic regions; it has, however, underestimated high-precipitation events. The TRMM data set is gridded in a monthly temporal resolution, with  $0.25^\circ$  by  $0.25^\circ$  global spatial resolution with a band extending from  $50^\circ\text{S}$  to  $50^\circ\text{N}$ . This data set is available from 1998 to 2015. The rainfall measuring instruments on the TRMM satellite include the Precipitation Radar (PR), electronically scanning radar operating at 13.8 GHz; TRMM Microwave Imager (TMI), a nine-channel passive microwave radiometer; and Visible and Infrared Scanner (VIRS), and a five channel visible/infrared radiometer. The algorithm combines multiple independent precipitation estimates from the TMI, Advanced Microwave Scanning Radiometer for Earth Observing Systems (AMSR-E), Special Sensor Microwave Imager (SSM/I), Special Sensor Microwave Imager/Sounder (SSMIS), Advanced Microwave Sounding Unit (AMSU), Microwave Humidity Sounder (MHS), microwave-adjusted merged geo-infrared (IR), and monthly GPCC rain gauge analysis.

After we identified deforested pixels for each year (see details in Supplemental Material), the next step was to understand how ET and  $P$  changed in deforested versus nearby intact forest areas, and test if there were any differences in their magnitudes for each year. For a deforested pixel of a given year  $t$ , we compared the central difference in annual accumulated ET and  $P$  between the following ( $t + 1$ ) and the previous ( $t - 1$ ) years as follows:

$$\delta ET_{t_i} = (ET)_{t_{i+1}} - (ET)_{t_{i-1}}, \quad (1)$$

$$\delta P_{t_i} = (P)_{t_{i+1}} - (P)_{t_{i-1}}, \quad (2)$$

where ET is the annual accumulated of MOD16 and  $P$  is the annual accumulated of TRMM. This approach (comparing  $t_{i+1}$  and  $t_{i-1}$  years to address changes before and after deforestation) was adopted because we could not establish when (at which month) the deforestation occurred in each pixel, we only know that it occurred on the  $t_i$  year.

This analysis was applied to all deforested, border and intact forest pixels within the basin. Then, we compared the average yearly change in ET and  $P$  of the deforested pixels against the border and intact forest pixels between 2000 and 2012. Following recommendations by Cox et al. (2013), for example, to disentangle the natural biophysical system from the perturbed system, we excluded the years 2005 and 2010 (as did Cox et al. (2013)) from the analysis because they were highly anomalous mega-drought years (Phillips et al. 2009; Lewis et al. 2011). For comparison, we show the results with all years included in the Supplemental Material. As our analysis is focused on the mean state of the hydrological regime, these anomalous records could mislead the deforestation change assessment at a fine scale.

We calculated the linear Pearson correlation between ET and  $P$  at each pixel on monthly, seasonal and yearly temporal scales for the period between 2000 and 2012. Furthermore, to address changes in the hydrological recycling ratio, we calculated the water recycling efficiency (WRE), which is the ratio between ET and  $P$  (details in Cowling et al. (2008)). WRE represents the percentage of precipitation returned to the atmosphere by ET from a given area. The WRE was calculated for the entire Amazon considering average ET and  $P$ , and also, WRE differences from 2012 to 2000 to evaluate if the water recycling has increased or decreased in the basin and at deforested areas.

This study evaluated the overall ET and  $P$  spatiotemporal changes in Amazon pixel-wise, regardless of from where the  $P$  comes from. Primarily because atmospheric moisture circulation is dynamic, the atmosphere is not a closed system, and different moisture sources and sinks could be associated with the  $P$  that falls over a region.

### 3. Results

To show how ET and  $P$  are coupled over the Amazon basin, we compiled a Pearson correlation map between  $P$  and ET using a monthly, seasonal, and yearly time step at 25 km resolution. The seasonal time step analysis showed the strongest correlation (Figure 1), and its spatial statistical significance was assessed through a chi-squared test (Figure S4 in Supplemental Material). We found a strong positive correlation over southern Amazonia, including areas mainly impacted by deforestation (detailed deforestation maps are shown in Figure S2 in the Supplemental Material) and of low absolute mean annual ET and  $P$  (Figures S8–S9). Our results show, with 99% confidence, that changes in ET correspond to changes in  $P$  in the same direction (i.e. increase in ET and increase in  $P$  or decrease in ET and decrease in  $P$ ). Nevertheless, over central and northern Amazonia, which is more densely vegetated and with wetland areas, the correlation in our analysis was strongly inversely correlated. The area in between these two sub-regions showed little correlation and poor statistical significance. Figure 1 shows the two distinct patterns that ET and  $P$  can assume depending on where they are being studied. As an illustration, Figure S5 in Supplemental Material shows the ET versus  $P$  scatter-plot for a deforested and intact forest region in the Amazon.

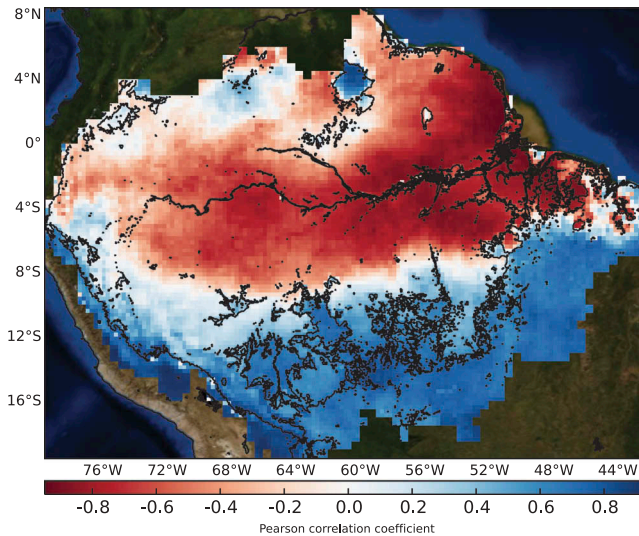


**Figure 1.** Seasonal Pearson correlation between evapotranspiration (ET) and precipitation ( $P$ ), at 25 km resolution. The 2012 deforestation is represented by a black contour. ET and  $P$  are shown to be strongly positively correlated in the southern Amazon basin, and strongly negatively correlated in the interior as remotely observed from MODIS and TRMM.

Because of the tropical humid Amazon climate, during the prolonged dry season in southern Amazonia an increase in biomass productivity is expected, especially at the beginning of the dry season as observed using remote sensing in Moura et al. (2015). In this sense, one could argue that a negative correlation between  $P$  and ET is expected in southern Amazonia; however, the highest (positive and negative) correlations among  $P$  and ET were found on a seasonal time step, which therefore do not capture isolated (monthly time) peak in vegetation productivity, but rather the dominant seasonal relationship between  $P$  and ET. As the focus of this study is on the impact of deforestation on the water cycle, this analysis focuses mostly on the deforested areas and the southern Amazonia. Thus, in the sequence, we analysed only the ET and  $P$  changes in deforested, borders, and intact forest pixel(s).

We evaluated annual ET and  $P$  between 2000 and 2012 along with the respective deforestation of each year. Figure 2 represents the time series of annual mean ET (orange) and  $P$  (blue) for deforestation (dot lines), border (dash lines), and intact forest (solid lines) areas and the regression lines based on an average of the three areas. We observe a slight increase in  $P$  and a greater increase in ET at and near deforested areas. ET in deforested areas increased from an average of 1110 mm in 2000 to 1299 mm in 2012, an increase of 17% in ET pixels (ANOVA:  $F = 133.9$ ,  $p$ -value  $< 0.001$ ).  $P$ , however, is more sensitive to drought years, which mask the increase of  $P$  over time, from 1902 mm in 2000 to 2023 mm in 2012, an increase of 6% (ANOVA:  $F = 29.0$ ,  $p$ -value  $< 0.01$ ).

In addition, as expected, ET and  $P$  absolute annual values are lower at deforested than intact forest areas. In 2012 ET was 6.9% lower (ANOVA:  $F = 144$ ,  $p$ -value  $< 0.001$ ) and  $P$  was 5.8% lower (ANOVA:  $F = 27.5$ ,  $p$ -value  $< 0.001$ ) in deforested areas in comparison to close intact forest areas. It is important to emphasize that this analysis was performed only for the deforested, border, and intact forest pixels and, therefore, it does not reflect

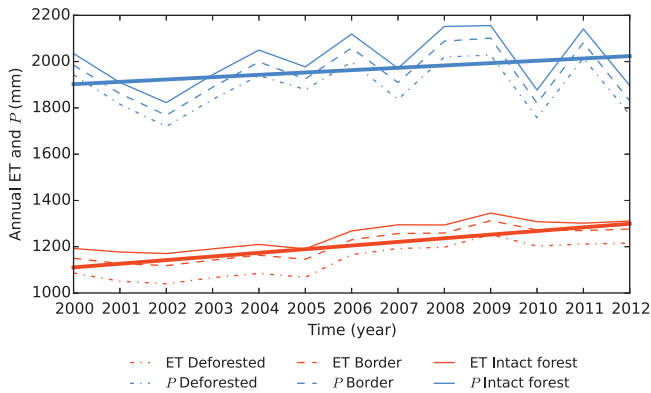


**Figure 2.** Annual evapotranspiration (ET) and precipitation ( $P$ ) time series from 2000 to 2012. ET and  $P$  have been increasing over time around Amazonian deforestation areas. Mean ET (orange) and average  $P$  (blue) in mm over deforested pixels (dot lines), border pixels (dash lines), and intact forest (solid line) pixels. The regression line is represented by the thicker line, which is an average of the three classes.

inferences for the entire amazon basin, but rather ET and  $P$  relative changes at the transitional zones. Discussion on the observed vegetation regrowth is presented in Figure S3 in the Supplemental Material.

To understand how ET and  $P$  values change in the deforested and intact forest areas, Figure 3 shows the mean change of ET (orange) and  $P$  (blue) over deforested pixels in Amazon, where the first two columns represent the mean change from the following year to the previous year (Equations (1) and (2)) for all deforested pixels within the basin and for the time period between 2000 and 2012 (excluding drought years: 2005 and 2010). Results with all years are shown in Figure S6 in the Supplemental Material.

Although absolute ET and  $P$  values are lower at the deforested areas in comparison to the border areas (Figure 2), in Figures 2 and 3 it is possible to observe, in general, a positive change in ET and  $P$  in the last 10 years. In Figure 3 this positive change is of 18.0 mm ( $\pm 3.9$ ), 21.6 mm ( $\pm 4.0$ ), 25.9 mm ( $\pm 4.0$ ) in  $P$  and 13.3 mm ( $\pm 1.2$ ), 11.6 mm ( $\pm 1.1$ ), 10.6 mm ( $\pm 1.1$ ) in ET over deforested, borders and intact forest, respectively. In terms of annual ET, these uncertainties agree with the mean error of  $11 \pm 6\%$  found by Ruhoff (2011) when validating annual ET of MOD16 against seven flux towers in Amazon basin.

The positive change in ET was 25.3% ( $p$ -value  $< 0.05$ ) greater in deforested relative to intact forest areas, which could be an outcome of mainly physical evaporation process and a lack of water retention over deforested land. This would cause precipitated water going directly to the atmosphere instead of infiltration or runoff, possibly due to the high surface temperatures and high heat of convection. In this sense, although Amazon deforested regions show lower absolute values of ET and  $P$ , the high heat of convection drives evaporation at non-saturated local air conditions, and thus induces evaporation as soon as precipitation occurs (positive correlation). This effect may have intensified over time given increases in global surface temperature – especially at the tropics.

$P$ , on other hand, shows a mean positive change 30.5% ( $p$ -value  $< 0.05$ ) smaller in deforested relative to intact forest areas. Although the coarse  $P$  data resolution ( $0.25^\circ$ ) masks strong changes in the forested–deforested profile, we interpret that  $P$  would be

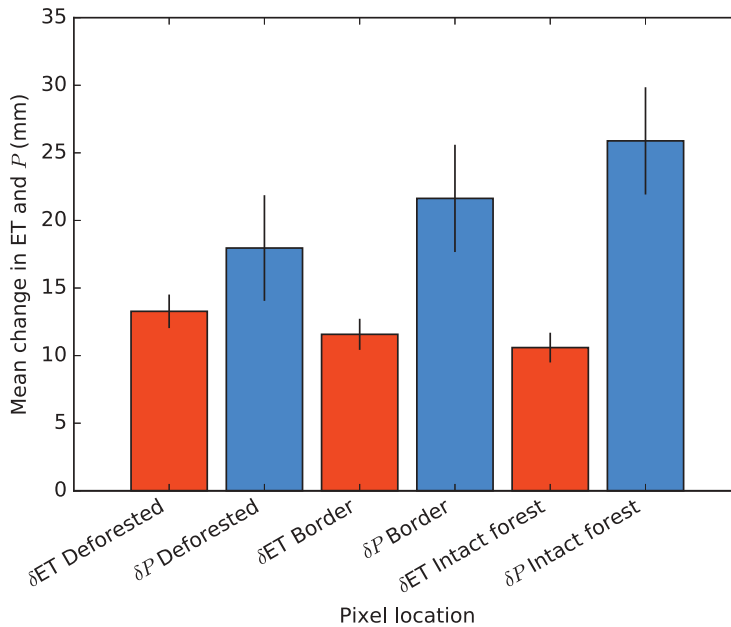


**Figure 3.** Mean change in evapotranspiration (ET) from MOD16 and precipitation ( $P$ ) from TRMM over deforested, border, and intact forest areas. The error bars shows the standard deviation. Positive changes in  $P$  are larger in intact forested areas than outside; oppositely, positive changes in ET are larger at deforested areas than inside forest.

increasing from outside to inside the forest, whereas ET would also be increasing in general, but from inside to outside the forest. The heterogeneous fishbone deforestation pattern observed in Amazonia can enhance the moisture gradient along the forest borders, and along with the strong heat of convection in the tropical areas, this can induce upward moisture circulation. Wang et al. (2009) found that heterogeneities in the land cover can generate shallow convection over the deforested areas, which are relatively more active than the deep convection over the forested areas. However, Wang et al. (2009) highlight that this strong lifting mechanism in deforested areas is caused by mesoscale circulations.

To demonstrate the relationship of mean absolute and mean changes in ET with the forest borders, in Figure S7 in Supplemental Material we show a comparison of mean annual ET, mean  $\delta ET$ , and the area/perimeter ratio of deforested areas. We found that the strongest positive change in ET is linked to deforested patches located at regions of more exposed borders (low area/perimeter ratio), and low absolute mean annual ET. This corroborates the assumption that high heat of convection at non-saturated air areas along with the border effect could be enhancing moisture convection at those regions.

For illustration of the spatial distribution of these ET and  $P$  changes, we show in Figure 4 absolute changes in ET and  $P$  from 2012 to 2000 over a box in northern and southern Amazonia. The deforestation of these boxes are represented in Figure 4(c) and Figure 4(d); absolute changes in ET are represented in Figure 4(e) and Figure 4(f), and absolute changes in  $P$  in Figure 4(g) and Figure 4(h). Values of ET are limited in 400 mm, therefore dark blue colour represent values of 400 mm or greater, likewise for the lower values in ET and in  $P$ .

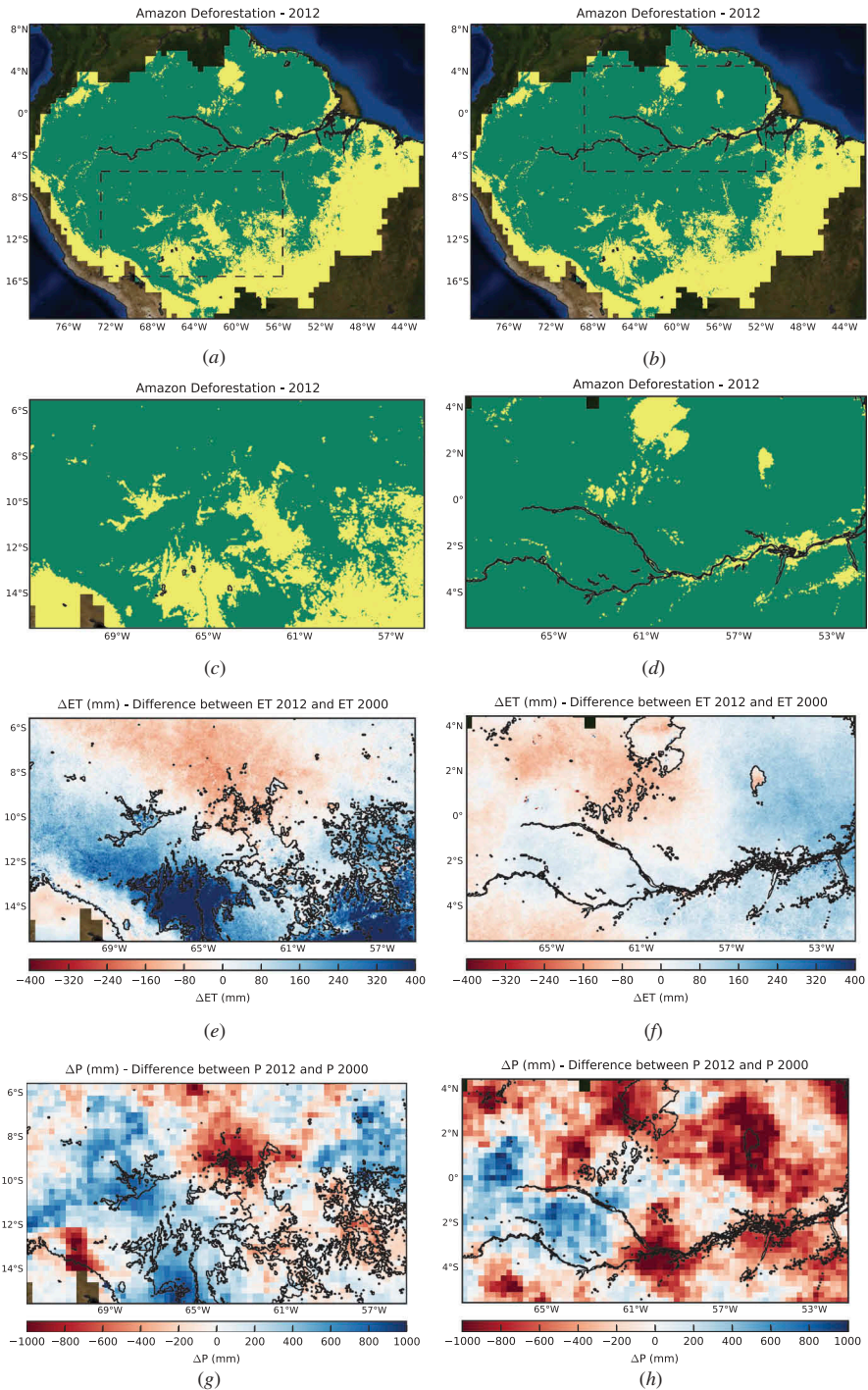


**Figure 4.** Absolute change in evapotranspiration (ET) and precipitation (P) from 2000 to 2012. Figures (a) and (b) represent the deforestation in Amazonia over 2012 (in green the forest areas, and in yellow the deforested areas); (c) and (d) a zoom-in Amazon deforestation over 2012. Figures (e) and (f) represent ET differences between 2012 and 2000 within the zoom area; and, (g) and (h) P differences between 2012 and 2000 within the zoom area. The 2012 deforestation is represented by a black contour.

When evaluating absolute changes in ET in [Figure 4](#) we observed a general increase of 19.5% ( $p$ -value < 0.001) over deforested areas particularly over southern Amazonia and a slight reduction of 2.75% ( $p$ -value < 0.001) in ET over vegetated areas. When analysing these absolute changes over the northern Amazonia, the pattern is weaker but with a small tendency of decreasing 0.32% ( $p$ -value < 0.05) ET over deforested areas; an increase of 1.37% ( $p$ -value < 0.05) in ET in the river flow and nearby could be associated with the increase of water availability to evaporate due to increasing in terrestrial water storage. Regarding absolute changes over  $P$ , the patterns are somewhat shifted due to atmospheric circulation and cloud mobility (D'Almeida et al. 2006). In [Figure 4\(e\)](#) and [Figure 4\(g\)](#) areas where there is an ET increase are spatially associated with areas where there is a  $P$  increase.

This relationship agrees with the positive correlation found in [Figure 1](#) over mainly deforested areas and southern Amazonia, especially in terms of ET. In northern Amazonia, however, the strong negative correlation between ET and  $P$  is mainly over forest areas, seen in [Figure 4\(f\)](#) and [Figure 4\(h\)](#). Areas with a slight increase of 1.37% ( $p$ -value < 0.05) in ET are associated with strong decreases of 22.3% ( $p$ -value < 0.001) in  $P$ . On the other hand, the deforested areas represented in [Figure 4\(f\)](#) and [Figure 4\(h\)](#) follow a positive correlation – in agreement with the correlation map – and show a decrease in ET and  $P$ .

[Figure 5](#) shows the mean annual WRE between 2000 and 2012 and [Figure 6](#) shows the difference between WRE from 2012 to 2000, both using ET and  $P$  from the same period (available, respectively, in [Figure S8](#) and [Figure S9](#) in the Supplemental Material). We find high WRE over the Amazon River, lakes and coastal areas due to strong heat of convection, high ET, and plenty of water availability over these areas. Near the Andes Mountains and northeast Brazil we found high WRE mainly because of high ET, low  $P$ , and high vapour pressure deficit in these areas. The WRE values vary between 45% and 110%; but even with the effects of high WRE over areas with high water availability to evaporate, we found an average WRE of  $62.3 \pm 17.0\%$ . Moreover, when evaluating WRE change from 2000 to 2012, WRE increase 28.9% ( $p$ -value < 0.001) in deforested areas and 17.5% ( $p$ -value < 0.001) in forest areas. The overall WRE increase of 21.1% ( $p$ -value < 0.001) in the Amazon implies that more water is being evaporated relative to the amount of water precipitated locally. Along with changes in land cover, Costa and Foley (1999) explain that this increase in internal water recycling could be associated with a decrease in atmospheric transport of water vapour in and out of Amazon.

## 4. Discussion

The Amazon rainforest is highly heterogeneous and tightly coupled to its surrounding atmospheric and hydrological cycling; thus, resolution of changes in ET and  $P$  with deforestation is non-trivial. The scientific community has made a lot of efforts to expand the understanding of these couplings, and now with the advances in remote-sensing measurements these intentions are more easily achievable.

Our results using remote sensing show a significant and correlated positive change in  $P$  and ET.  $P$  showed a slight positive change over deforested pixels and even more over intact forest pixels. Meanwhile, ET showed a consistent and significant positive change over deforested in comparison to intact forested pixels. These results disagree with macroscale climate models that simulate reduction in regional

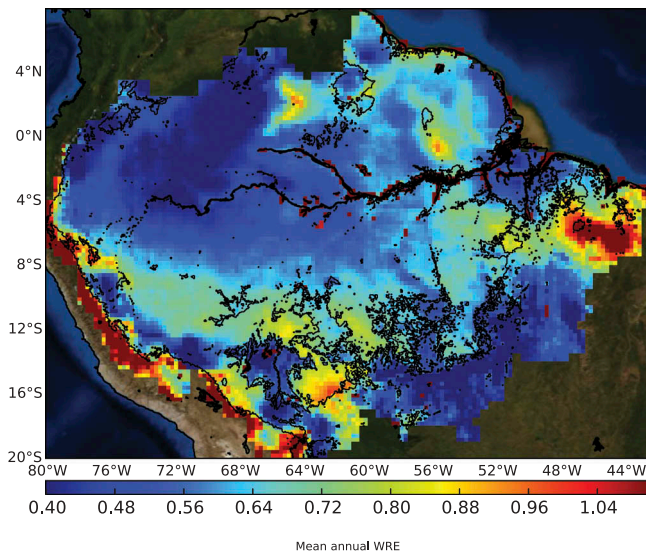


**Figure 5.** Mean water recycling efficiency (WRE) from 2000 to 2012. The 2012 deforestation is represented by a black contour.

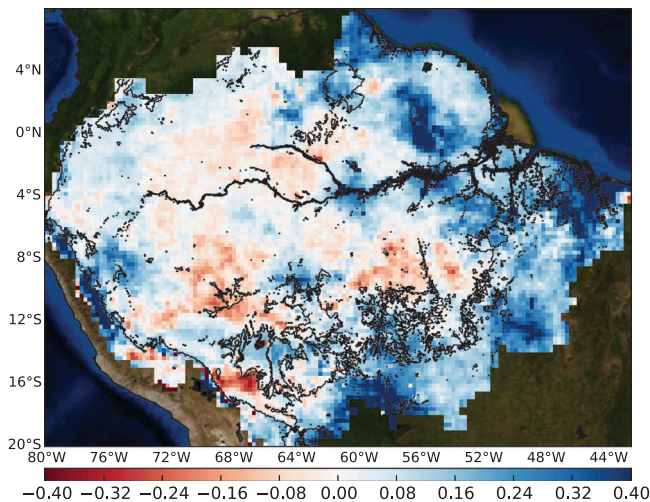


**Figure 6.** The water recycling efficiency (WRE) difference from 2012 to 2000. The 2012 deforestation is represented by a black contour. We found a slight increase in WRE with deforestation.

precipitation as a result of tropical deforestation at large-scale. (Eltahir and Bras 1996; Shukla, Nobre, and Sellers 1990). However, our results agree with mesoscale models and observational studies that have linked tropical deforestation to relative increase in precipitation locally (Butt, de Oliveira, and Costa 2011; Ometto et al. 2005; D’Almeida et al. 2006). Moreover, we found a significant highly positive correlation between seasonal ET and  $P$  over southern Amazon, which coincides with where the deforestation has occurred.

D'Almeida et al. (2006) explained that positive or negative changes in  $P$  are associated with the spatial scale and the heterogeneity of the area. Furthermore, size and fragmentation of the disturbed regions can determine whether the water cycle in the basin becomes intensified or weakened under particular deforestation scenarios. This mechanism has been studied before using mesoscale models in Amazonia: Avissar et al. (2002) and Ometto et al. (2005) found a threshold of extent and distribution at which deforestation leads to a local increase or decrease in  $P$ . Furthermore, Garcia-Carreras and Parker (2011) found that  $P$  can be 4–6 times higher over heterogeneous warmer surface compared to a homogeneous surface.

The fishbone deforestation pattern cut out of Amazonia acts as a forest opening up that allows moisture to escape more easily from the below canopy layer as air circulation is improved. The forest glades can intensify the horizontal heat flux gradient between disturbed and undisturbed areas, which can trigger thermally generated mesoscale circulations (Roy 2009) characterized by increases in sensible heat fluxes in the deforested regions (Khanna and Medvigy 2014). This system has the potential to create anomalous convective circulations cells and turbulent zones that boost moisture convergence, enhancing clouds formation and water vapour convergence (Garcia-Carreras and Parker 2011; Negri et al. 2004). Likewise, changes in circulations may significantly affect the timing and formation of clouds, potentially altering both intensity and distribution of  $P$  (Chen and Avissar 1994; Marengo and Nobre 2001). Additionally, possibilities for the increase in  $P$  over deforested areas can be associated with a southward shift of intertropical convergence zone (ITCZ) (Costa and Foley 1997), as well as changes in the sea surface temperature, and oceanic moisture inflow and outflow patterns (Costa and Foley 1999). Nevertheless, this enhanced  $P$  over deforested border areas can act as a negative feedback by improving regeneration of the forest (Garcia-Carreras and Parker 2011).

Accordingly, the influence of the size and heterogeneity of deforestation pattern, as explained by D'Almeida et al. (2006), and the land interactions with the local climate (hot and humid) lead to the main differences between the macroscale and the mesoscale models. One of the advantages of the macroscale models is the ability to calculate both large and mesoscale dynamics, the finer-scale thermodynamics processes, and their associated feedback. However, macroscale models predict reductions in  $P$ , ET, moisture convergence, and runoff with deforestation, along with long-term increase in surface temperature (Eltahir and Bras 1996). These models are not well equipped to simulate the heterogeneities of the small-scale deforestation, or estimates that accurately produce the effects of such deforestation on ET and  $P$  (Correia, Alvalá, and Manzi 2008).

The parameterizations employed by the current generation of atmospheric general circulation models (GCM) tend to rely only on the quantification of turbulence effects, neglecting the influence of the heat fluxes associated with anomalous mesoscale circulations (Roy and Avissar 2002), which are essential for thermally driven circulations. Stone and Risbey (1990) reported that macroscale heat fluxes interact so strongly with the parameterized subgrid-scale physics that their calculations of large-scale fluxes are no more accurate than their calculation of subgrid-scale physics. Stone and Risbey (1990) found that meridional transport of heat simulated by GCM used in climate change experiments differs from observational analyses and from other GCM by as much as a factor of 2. Regarding possible physical reasons, Davidson et al. (2012)

reported that at deforestation scales greater than  $10^5 \text{ km}^2$  there will be a tendency to decrease  $P$  because of a decrease in the ET in deforested regions, and this results in a downwind transport of the water vapour. Also, decreases in  $P$  for large-scale deforestation could be associated with decreases in absorbed net solar energy and a consequent general weakening of the continental-scale low-pressure system that drives precipitation over the basin (Davidson et al. 2012). Thus, despite the specific importance of expanding the understanding of the large-scale processes, these sets of models alone are inappropriate to simulate hydroclimate changes over deforestation in Amazonia.

Given that we also found positive changes of  $P$  and ET over deforested pixels using remotely sensed data at 25 km resolution, as it was seen in Figures 2 and 3, we support the mesoscale models as the best representations of changes in ET and  $P$  when simulating impacts of deforestation in Amazonia. Moreover, mesoscale models suggest an increase in convection and potential  $P$  along the borders between forest and deforested/urban areas, and  $P$  at regional scales depending on the deforestation extent (Roy and Avissar 2002). When analysing long-term absolute differences in ET and  $P$  (Figure 4), it was clear that the positive changes in  $P$  and ET over southern Amazonia occurred mainly where the patched vegetation distribution follows a positive ET– $P$  correlation. Meanwhile, in northern Amazonia, where the vegetation pattern is homogeneous, a smaller positive change in  $P$  and a larger positive change in ET was predominant, following a significant negative ET– $P$  correlation. This, along with the border ratio analysis presented in Figure S7, agrees with the findings of Garcia-Carreras and Parker (2011) on  $P$  differences over homogeneous versus heterogeneous warmer areas.

The mesoscale models can assess finer-scale land–atmosphere feedback that are not accurately resolved by models with much coarser spatial resolutions ( $>10^2 \text{ km}^2$ ). Also, mesoscale models can detect anomalous circulations induced by air temperature contrasts over regions of extreme land surface gradients in different parts of the globe. The presence of patches over Amazonia increase the area of borders, which according to Camargo and Kapos (1995) have higher soil moisture, and vapour pressure deficit (VPD) increases with height near the edges. On these border areas there are more leaves, more ET, and depleted moisture, thus protecting forest edges from desiccating. Moreover, the interaction between mesoscale circulations induced by land surface heterogeneities and the large-scale flow, together, can enhance and deepen the convective activity over disturbed areas (Roy and Avissar 2002).

We acknowledge the limitations of remote-sensing products for studies of the land surface. While most remote-sensing products are imperfect, it is crucial that uncertainties are documented and characterized for application to scientific inquiry. For instance, the MOD16 ET data carry a well-characterized uncertainty of  $11 \pm 6\%$  within extensive and independent evaluations from flux sites throughout Amazonia and from multiple papers (Ruhoff 2011; Trambauer et al. 2014). Hence, our line of inquiry must be statistically evaluated with these uncertainties being accounted for, thereby enabling the detection of differences in such uncertainties. Thus, we report our findings with confidence within an uncertainty bound of  $11 \pm 6\%$ .

With respect to the Amazon WRE ratio, Marengo (2005) assert that, over Amazonia,  $P$  exceeds ET and the basin acts as a sink of moisture ( $P > ET$ ). However, there are some occasions where the basin can act as a source for moisture ( $P < ET$ ). Keys, Wang-Erlandsson, and Gordon (2016) used the ERA-Interim reanalysis data set and land-cover type from MODIS

to assess global vegetation-regulated moisture recycling. They found  $P$  to be vegetation-regulated, due to inland and downwind land ET in southern Amazonia, and  $P$  is shown to be mostly by downwind land ET regulated in northeastern Amazonia. We found that the WRE values can vary spatially between 45% and 110%, which shows that some areas in Amazonia that have high WRE, which can act as a source of moisture. Moreover, Marengo and Nobre (2001), using a GCM, found that 63% and 73% of the annual  $P$  is evapotranspired, whereas using MOD16 ET and TRMM  $P$ , even with the effects of high WRE over areas with high water availability to evapotranspire, we found an average of  $62.3\% \pm 17.0\%$ , which is very similar to that modelled by Marengo and Nobre (2001).

Although we focus on  $P$  recycling from ET, Burde, Gandush, and Yunden (2006) explain that  $P$  recycling does not drive  $P$ , as  $P$  is largely determined fundamentally by large-scale atmospheric circulation, which in turn is driven by differential atmospheric heating. Thus,  $P$  acts as a feedback because energy input is necessary to induce large-scale circulation that sustains  $P$ , so a consistent treatment of the column and surface energy budget may be crucial. Therefore, even though we found a positive change in ET and  $P$  over southern Amazonia deforested regions this should be interpreted as only a feedback of the heterogeneous warmer land–atmosphere interaction with ET and  $P$ , not a statement on  $P$  recycling for Amazonia at large.

## 5. Conclusions

The main goal of this analysis using MOD16 ET and TRMM  $P$  was to assess the changes in the hydrological dynamics due to deforestation in Amazon using satellite observations. We found a positive change in ET and  $P$  over border deforested areas, mainly located in southern Amazonia. The change in ET was larger outside in comparison to inside of forest; meanwhile,  $P$  increased more from inside intact forest areas to the borders. These results agree with mesoscale rather than macroscale models, as the former are able to capture finer-scale land–atmosphere heat fluxes and feedback over heterogeneous patches of deforestation in non-saturated air condition Amazon regions. Moreover, the correlation between ET and  $P$  varies according to the location and climatic dynamic patterns over certain sub-regions within Amazonia. Although the period of study was decadal rather than climatic, and there are limitations with some of the remote-sensing data, satellite observations have demonstrated to be a powerful tool to assess changes due to deforestation at heterogeneous and dynamic regions as Amazonia, and expand our understanding of the processes involved.

## Acknowledgements

We thank the Brazilian government through CAPES (Coordenacao de Aperfeicoamento de Pessoal de Nivel Superior) for the Brazil Science Without Borders programme scholarship. We thank K. Mallick for support with data set acquisition, and meaningful collaboration through discussions and suggestions on this analysis; and M. Gobbi for support from Federal University of Parana. We also thank friends for various support: R. Lopes, M. Sikka, M. Shi, M. Sok. The MODIS data is available at <http://www.ntsug.umd.edu/project/mod16>, and TRMM data at [http://disc.gsfc.nasa.gov/datacollection/TRMM\\_3B43\\_V7.html](http://disc.gsfc.nasa.gov/datacollection/TRMM_3B43_V7.html). The research was carried out at the Jet Propulsion Laboratory, California Institute of Technology, under a contract with the National Aeronautics and Space Administration. Copyright 2016 California Institute of Technology. Government sponsorship acknowledged.

## Disclosure statement

No potential conflict of interest was reported by the authors.

## Funding

This work was supported by the Coordenação de Aperfeiçoamento de Pessoal de Nível Superior [grant number 6250/12-2].

## ORCID

Noemi Vergopolan  <http://orcid.org/0000-0002-7298-0509>

Joshua B. Fisher  <http://orcid.org/0000-0003-4734-9085>

## References

- Aragao, L. E. O. C., Y. Malhi, N. Barbier, A. Lima, Y. Shimabukuro, L. Anderson, and S. Saatchi. 2008. "Interactions between Rainfall, Deforestation and Fires during Recent Years in the Brazilian Amazonia." *Philosophical Transactions of the Royal Society B: Biological Sciences* 363 (1498): 1779–1785. doi:10.1098/rstb.2007.0026.
- Avissar, R., P. L. Silva Dias, M. A. F. Silva Dias, and C. Nobre. 2002. "The Large-Scale Biosphere-Atmosphere Experiment in Amazonia (LBA): Insights and Future Research Needs." *Journal of Geophysical Research: Atmospheres (1984-2012)* 107 (D20): LBA 54–1–LBA 54–6.
- Azarderakhsh, M., W. B. Rossow, F. Papa, H. Norouzi, and R. Khanbilvardi. 2011. "Diagnosing Water Variations within the Amazon Basin Using Satellite Data." *Journal of Geophysical Research: Atmospheres* 116 (D24): D24107. doi:10.1029/2011JD015997.
- Burde, G. I., C. Gandush, and B. Yunden. 2006. "Bulk Recycling Models with Incomplete Vertical Mixing. Part II: Precipitation Recycling in the Amazon Basin." *Journal of Climate* 19 (8): 1473–1489. ID: 441415376. doi:10.1175/JCLI3688.1
- Butt, N., P. A. de Oliveira, and M. H. Costa. 2011. "Evidence that Deforestation Affects the Onset of the Rainy Season in Rondonia, Brazil." *Journal of Geophysical Research: Atmospheres (1984-2012)* 116 (D11). doi:10.1029/2010JD015174.
- Camargo, J. L. C., and V. Kapos. 1995. "Complex Edge Effects on Soil Moisture and Microclimate in Central Amazonian Forest." *Journal of Tropical Ecology* 11 (2): 205–221. doi:10.1017/S026646740000866X.
- Chen, F., and R. Avissar. 1994. "Impact of Land-Surface Moisture Variability on Local Shallow Convective Cumulus and Precipitation in Large-Scale Models." *Journal of Applied Meteorology* 33 (12): 1382–1401. doi:10.1175/1520-0450(1994)033<1382:IOLSMV>2.0.CO;2.
- Correia, F. W. S., R. C. S. Alvalá, and A. O. Manzi. 2008. "Modeling the Impacts of Land Cover Change in Amazonia: A Regional Climate Model (RCM) Simulation Study." *Theoretical and Applied Climatology* 93 (3–4): 225–244. doi:10.1007/s00704-007-0335-z.
- Costa, M. H., and J. A. Foley. 1997. "Water Balance of the Amazon Basin: Dependence on Vegetation Cover and Canopy Conductance." *Journal of Geophysical Research: Atmospheres* 102 (D20): 23973–23989. doi:10.1029/97JD01865.
- Costa, M. H., and J. A. Foley. 1999. "Trends in the Hydrologic Cycle of the Amazon Basin." *Journal of Geophysical Research. D. Atmospheres* 104: 14189–14198. doi:10.1029/1998JD200126.
- Costa, M. H., and G. F. Pires. 2010. "Effects of Amazon and Central Brazil Deforestation Scenarios on the Duration of the Dry Season in the Arc of Deforestation." *International Journal of Climatology* 30 (13): 1970–1979. doi:10.1002/joc.2048.
- Cowling, S. A., Y. Shin, E. Pinto, and C. D. Jones. 2008. "Water Recycling by Amazonian Vegetation: Coupled versus Uncoupled Vegetation–Climate Interactions." *Philosophical Transactions of the Royal Society B: Biological Sciences* 363 (1498): 1865–1871. doi:10.1098/rstb.2007.0035.

- Cox, P. M., D. Pearson, B. B. Booth, P. Friedlingstein, C. Huntingford, C. D. Jones, and C. M. Luke. 2013. "Sensitivity of Tropical Carbon to Climate Change Constrained by Carbon Dioxide Variability." *Nature* 494 (7437): 341–344. doi:10.1038/nature11882.
- D'Almeida, C., C. J. Vorosmarty, J. A. Marengo, G. C. Hurtt, S. L. Dingman, and B. D. Keim. 2006. "A Water Balance Model to Study the Hydrological Response to Different Scenarios of Deforestation in Amazonia." *Journal of Hydrology* 331 (1–2): 125–136. doi:10.1016/j.jhydrol.2006.05.027.
- D'Almeida, C., C. J. Vrsmary, G. C. Hurtt, J. A. Marengo, S. L. Dingman, and B. D. Keim. 2007. "The Effects of Deforestation on the Hydrological Cycle in Amazonia: A Review on Scale and Resolution." *International Journal of Climatology* 27 (5): 633–647. doi:10.1002/joc.1475.
- Davidson, E. A., A. C. de Araujo, J. K. Paulo Artaxo, I. F. Balch, M. M. Brown, C. Bustamante, M. T. Coe, et al. 2012. "The Amazon Basin in Transition." *Nature* 481(7381): 321–328. M3: 10.1038/nature10717. doi:10.1038/nature10717.
- Dickinson, R. E., and P. Kennedy. 1992. "Impacts on Regional Climate of Amazon Deforestation." *Geophysical Research Letters* 19 (19): 1947–1950. doi:10.1029/92GL01905.
- Eltahir, E. A. B., and R. L. Bras. 1996. "Precipitation Recycling." *Reviews of Geophysics* 34 (3): 367–378. ID: 207980085. doi:10.1029/96RG01927
- Fisher, J. B., Y. Malhi, D. Bonal, H. R. Da Rocha, A. C. De Araujo, M. Gamo, M. L. Goulden et al. 2009. "The Land–Atmosphere Water Flux in the Tropics." *Global Change Biology* 15 (11): 2694–2714. doi:10.1111/j.1365-2486.2008.01813.x.
- Garcia-Carreras, L., and D. J. Parker. 2011. "How Does Local Tropical Deforestation Affect Rainfall?" *Geophysical Research Letters* 38: 19. doi:10.1029/2011GL049099.
- Huete, A., K. Didan, T. Miura, E. Patricia Rodriguez, X. Gao, and L. G. Ferreira. 2002. "Overview of the Radiometric and Biophysical Performance of the MODIS Vegetation Indices." *Remote Sensing of Environment* 83 (1): 195–213. doi:10.1016/S0034-4257(02)00096-2.
- Huete, A., K. Didan, Y. Shimabokuro, L. Ferreira, and E. Rodriguez. 2000. "Regional Amazon Basin and Global Analyses of MODIS Vegetation Indices: Early Results and Comparisons with AVHRR." Geoscience and Remote Sensing Symposium, Honolulu, HI, 2000. Proceedings. IGARSS 2000. IEEE 2000, Vol. 2536–2538. IEEE. Available from: <http://ieeexplore.ieee.org/document/861621/>
- Karaseva, M. O., S. Prakash, and R. M. Gairola. 2012. "Validation of High-Resolution TRMM-3B43 Precipitation Product Using Rain Gauge Measurements over Kyrgyzstan." *Theoretical and Applied Climatology* 108 (1–2): 147–157. doi:10.1007/s00704-011-0509-6.
- Keys, P. W., L. Wang-Erlandsson, and L. J. Gordon. 2016. "Revealing Invisible Water: Moisture Recycling as an Ecosystem Service." *PLoS ONE* 11 (3): 1–16. doi:10.1371/journal.pone.0151993.
- Khanna, J., and D. Medvigy. 2014. "Strong Control of Surface Roughness Variations on the Simulated Dry Season Regional Atmospheric Response to Contemporary Deforestation in Rondônia, Brazil." *Journal of Geophysical Research: Atmospheres* 119 (23): 13–067.
- Knipper, K. R., A. M. Kinoshita, and T. S. Hogue. 2016. "Evaluation of a Moderate Resolution Imaging Spectroradiometer Triangle-Based Algorithm for Evapotranspiration Estimates in Subalpine Regions." *Journal of Applied Remote Sensing* 10 (1): 016002–016002. doi:10.1117/1.JRS.10.016002.
- Knox, R., G. Bisht, J. Wang, and R. Bras. 2011. "Precipitation Variability over the Forest-To-Nonforest Transition in Southwestern Amazonia." *Journal of Climate* 24 (9): 2368–2377. doi:10.1175/2010JCLI3815.1.
- Lewis, S. L., P. M. Brando, O. L. Phillips, G. M. Der Heijden Van, and D. Nepstad. 2011. "The 2010 Amazon Drought." *Science* 481 (7381): 321–328. doi:10.1126/science.1200807.
- Los, S. O. 1999. "A Global Multi-Year Biophysical Land Surface Data Set from NOAA AVHRR Data." Geoscience and Remote Sensing Symposium, Hamburg, 1999. IGARSS'99 Proceedings. IEEE 1999, Vol. 21087–1089. IEEE. <http://ieeexplore.ieee.org/document/774541/>
- Marengo, J. A., B. Liebmann, A. M. Grimm, V. Misra, P. L. Silva Dias, I. F. A. Cavalcanti, L. M. V. Carvalho, et al. 2012. "Recent Developments on the South American Monsoon System." *International Journal of Climatology* 32 (1): 1–21. doi:10.1002/joc.2254.

- Marengo, J. A. 2005. "Characteristics and Spatio-Temporal Variability of the Amazon River Basin Water Budget." *Climate Dynamics* 24 (1): 11–22. J2: Clim Dyn. doi:10.1007/s00382-004-0461-6.
- Marengo, J. A., and C. A. Nobre. 2001. "General Characteristics and Variability of Climate in the Amazon Basin and Its Links to the Global Climate System." *The Biogeochemistry of the Amazon Basin* 2: 17–41.
- Medvigy, D., R. L. Walko, M. J. Otte, and R. Avissar. 2013. "Simulated Changes in Northwest US Climate in Response to Amazon Deforestation." *Journal of Climate* 26 (22): 9115–9136. doi:10.1175/JCLI-D-12-00775.1.
- Miralles, D. G., C. Jiménez, M. Jung, D. Michel, A. Ershadi, M. F. McCabe, M. Hirschi, et al. 2015. The WACMOS-ET Project-Part 2: Evaluation of Global Terrestrial Evaporation Data Sets. *Hydrology & Earth System Sciences Discussions* 12(10): doi:10.5194/hessd-12-10651-2015.
- Molinari, J., and M. Dudek. 1992. "Parameterization of Convective Precipitation in Mesoscale Numerical Models: A Critical Review." *Monthly Weather Review* 120 (2): 326–344. doi:10.1175/1520-0493(1992)120<0326:POCPIM>2.0.CO;2.
- Monteith, J. L. 1965. "Evaporation and Environment." In *Symposia of the Society for Experimental Biology*, Vol. 19205–234. London: Society for Experimental Biology. <http://www.unc.edu/courses/2007fall/geog/801/001/www/ET/Monteith65.pdf>
- Moura, Y. M., T. Hilker, A. I. Lyapustin, L. S. Galvão, J. R. Dos Santos, L. O. Anderson, C. H. R. De Sousa, and E. Arai. 2015. "Seasonality and Drought Effects of Amazonian Forests Observed from Multi-Angle Satellite Data." *Remote Sensing of Environment* 171: 278–290. doi:10.1016/j.rse.2015.10.015.
- Mu, Q., M. Zhao, and S. W. Running. 2011. "Improvements to a MODIS Global Terrestrial Evapotranspiration Algorithm." *Remote Sensing of Environment* 115 (8): 1781–1800. doi:10.1016/j.rse.2011.02.019.
- Mu, Q., F. A. Heinsch, M. Zhao, and S. W. Running. 2007. "Development of a Global Evapotranspiration Algorithm Based on MODIS and Global Meteorology Data." *Remote Sensing of Environment* 111 (4): 519–536.
- Negri, A. J., R. F. Adler, X. Liming, and J. Surratt. 2004. "The Impact of Amazonian Deforestation on Dry Season Rainfall." *Journal of Climate* 17 (6): 1306–1319. doi:10.1175/1520-0442(2004)017<1306:TIOADO>2.0.CO;2.
- Nobre, P., D. F. Marta Malagutti, R. A. Urbano, F. De Almeida, and E. Giarolla. 2009. "Amazon Deforestation and Climate Change in a Coupled Model Simulation." *Journal of Climate* 22 (21): 5686–5697. M3: Article. doi:10.1175/2009JCLI2757.1
- Ometto, J. P. H. B., A. D. Nobre, H. R. Rocha, P. Artaxo, and L. A. Martinelli. 2005. "Amazonia and the Modern Carbon Cycle: Lessons Learned." *Oecologia* 143 (4): 483–500. doi:10.1007/s00442-005-0034-3.
- Phillips, O. L., L. E. O. C. Aragão, S. L. Lewis, J. B. Fisher, J. Lloyd, G. López-González, Y. Malhi, et al. 2009. "Drought Sensitivity of the Amazon Rainforest." *Science* 323 (5919): 1344–1347. doi:10.1126/science.1164033.
- Pokam, W., L. Djotang, and F. Mkankam. 2012. "Atmospheric Water Vapor Transport and Recycling in Equatorial Central Africa through NCEP/NCAR Reanalysis Data." *Climate Dynamics* 38 (9–10): 1715–1729. doi:10.1007/s00382-011-1242-7.
- Ramos da Silva, R., and R. Avissar. 2006. "The Hydrometeorology of a Deforested Region of the Amazon Basin." *Journal of Hydrometeorology* 7 (5): 1028–1042. doi:10.1175/JHM537.1.
- Ramos da Silva, R., D. W. Renato, and R. Avissar. 2008. "Regional Impacts of Future Land-Cover Changes on the Amazon Basin Wet-Season Climate." *Journal of Climate* 21 (6): 1153–1170. doi:10.1175/2007JCLI1304.1.
- Randow, R. C. S, C. von Randow, R. W. A. Hutjes, J. Tomasella, and B. Kruijt. 2012. "Evapotranspiration of Deforested Areas in Central and Southwestern Amazonia." *Theoretical and Applied Climatology* 109 (1–2): 205–220. doi:10.1007/s00704-011-0570-1.
- Roy, S. B. 2009. "Mesoscale Vegetation-Atmosphere Feedbacks in Amazonia." *Journal of Geophysical Research: Atmospheres (1984–2012)* 114 (D20). doi:10.1029/2009JD012001.

- Roy, S. B., and R. Avissar. 2002. "Impact of Land Use/Land Cover Change on Regional Hydrometeorology in Amazonia." *Journal of Geophysical Research: Atmospheres* 107 (D20): LBA 4–1–LBA 4–12.
- Ruhoff, A. L. 2011. "Sensoriamento remoto aplicado à estimativa da evapotranspiração em biomas tropicais." Ph.D. thesis. Universidade Federal do Rio Grande do Sul, Porto Alegre, Brazil. <http://www.lume.ufrgs.br/handle/10183/32468>.
- Ruhoff, A. L., L. E. O. C. Aragão, W. Collischonn, H. R. Da Rocha, Y. Malhi, Q. Mu, and S. Running 2013a. "Modelagem da evapotranspiração em áreas de floresta tropical amazônica." In *Anais*, J. C. N. Epiphany and L. S. Galvão edited by, 5459–5466. Simpósio Brasileiro de Sensoriamento Remoto, 16. (SBSR). São José dos Campos: Instituto Nacional de Pesquisas Espaciais (INPE). <http://urlib.net/dpi.inpe.br/marte2/2013/05.29.00.51.07>.
- Ruhoff, A. L., A. R. Paz, L. E. O. C. Aragao, Q. Mu, Y. Malhi, W. Collischonn, H. R. Rocha, and S. W. Running. 2013b. "Assessment of the MODIS Global Evapotranspiration Algorithm Using Eddy Covariance Measurements and Hydrological Modelling in the Rio Grande Basin." *Hydrological Sciences Journal* 58 (8): 1658–1676. doi:10.1080/02626667.2013.837578.
- Shukla, J., C. Nobre, and P. Sellers. 1990. "Amazon Deforestation and Climate Change." *Science* 247 (4948): 1322–1325. SE: New Series 10.1126/science.247.4948.1322.
- Soares-Filho, B. S., D. C. Nepstad, L. M. Curran, G. C. Cerqueira, R. A. Garcia, C. A. Ramos, E. Voll, A. McDonald, P. Lefebvre, and P. Schlesinger. 2006. "Modelling Conservation in the Amazon Basin." *Nature* 440 (7083): 520–523. doi:10.1038/nature04389.
- Spracklen, D. V., S. R. Arnold, and C. M. Taylor. 2012. "Observations of Increased Tropical Rainfall Preceded by Air Passage over Forests." *Nature* 489 (7415): 282–285. doi:10.1038/nature11390.
- Srivastava, P. K., D. Han, T. Islam, G. P. Petropoulos, M. Gupta, and Q. Dai. 2016. "Seasonal Evaluation of Evapotranspiration Fluxes from MODIS Satellite and Mesoscale Model Downscaled Global Reanalysis Datasets." *Theoretical and Applied Climatology* 124 (1–2): 461–473.
- Stone, P. H., and J. S. Risbey. 1990. "On the Limitations of General Circulation Climate Models." *Geophysical Research Letters* 17 (12): 2173–2176. doi:10.1029/GL017i012p02173.
- Sun, Z., Q. Wang, Z. Ouyang, M. Watanabe, B. Matsushita, and T. Fukushima. 2007. "Evaluation of MOD16 Algorithm Using MODIS and Ground Observational Data in Winter Wheat Field in North China Plain." *Hydrological Processes* 21 (9): 1196–1206. doi:10.1002/hyp.6679.
- Trambauer, P., E. Dutra, S. Maskey, M. Werner, F. Pappenberger, L. P. H. Van Beek, and S. Uhlenbrook. 2014. "Comparison of Different Evaporation Estimates over the African Continent." *Hydrology and Earth System Sciences* 18 (1): 193–212. doi:10.5194/hess-18-193-2014.
- Wang, J., F. J. F. Chagnon, E. R. Williams, A. K. Betts, N. O. Renno, L. A. T. Machado, G. Bisht, R. Knox, and R. L. Bras. 2009. "Impact of Deforestation in the Amazon Basin on Cloud Climatology." *Proceedings of the National Academy of Sciences* 106 (10): 3670–3674. doi:10.1073/pnas.0810156106.